

Continuum random-phase approximation for (n, γ) reactions on neutron-rich nuclei: collective effects and resonances

Teruyuki Saito

*Graduate School of Science and Technology,
Niigata University, Niigata 950-2181, Japan*

Masayuki Matsuo

Department of Physics, Faculty of Science. Niigata University, Niigata 950-2181, Japan

Abstract

We formulate a microscopic theory to calculate cross section of the radiative neutron capture reaction on neutron-rich nuclei using the continuum random-phase approximation (cRPA) to the time-dependent density functional theory (TDDFT). With an intension of applying to the r-process, for which the statistical reaction model may not be appropriate, we describe the transition between a initial state of incident neutron and a final state of the gamma decay by means of a single many-body framework of the cRPA-TDDFT. With the cRPA approach, it is possible to describe various excitation modes present in the (n, γ) reaction, including soft dipole excitation, the giant resonances as well as non-collective excitations and the single-particle resonances. Furthermore, it enables us to describe the (n, γ) reaction where the the final states of the gamma transition are low-lying surface vibrational states. We demonstrate the theory by performing numerical calculation for the reaction $^{139}\text{Sn}(n, \gamma)^{140}\text{Sn}$. We discuss various new features which are beyond the single-particle model; presence of narrow and wide resonances originating from non-collective and collective excitations and roles of low-lying quadrupole and octupole vibrational states.

I. INTRODUCTION

The r-process is believed to be the origin of about half of the elements heavier than iron [1–3]. From the viewpoint of nuclear physics, the nucleosynthesis is a complex network of the (n, γ) and (γ, n) reactions, the beta decay and the fission taking place on a large number of short-lived neutron-rich nuclei very far from the stability line. The cross sections and the probabilities of the relevant reactions and decays need to be provided theoretically for quantitative understanding since the direct experimental measurements are quite difficult or impossible in most cases. Recent observation of kilonova associated with a binary neutron star merger [4, 5] provides a first direct evidence and quantitative information on the r-process nucleosynthesis [3, 6–8]. It is therefore quite important for nuclear theory to provide reliable theoretical models of the relevant nuclear reactions which takes into account the recent progress of study of neutron-rich nuclei.

In the present study, we focus on the radiative neutron capture reactions. It is usually described in terms of two different mechanisms, the compound nuclear (CN) process and direct capture (DC) process [2, 3]. The CN process is assumed to proceed via compound states with high level density, and it is usually evaluated by means of the Hauser and Feshbach statistical model [9]. It is relevant for nuclei with relatively large neutron separation energy and and often applied to the s-process which occurs on stable nuclei or nuclei close to the stability line. The r-process path, however, lies on short-lived neutron-rich nuclei in which the neutron separation energy or the excitation energy of nuclei is as small as ~ 2 MeV, In this case the statistical description of the CN process may not be appropriate [2, 3, 10]. Often considered in this case is the direct capture process [10–21], where a neutron scattering state decays directly to a bound state without forming compound states. It is essentially a single-particle model of gamma decay or an independent-particle shell model for the nuclear structure.

There exists various nuclear structure phenomena beyond the single-particle description, such as the pairing correlation, the low-lying collective states, and giant resonances. In addition, neutron-rich nuclei far from the stability line exhibits characteristic features such as the neutron halo, the neutron skin and related exotic modes such as the pygmy dipole resonance or the soft dipole mode [22–27] originating from small neutron separation energy or the weak binding of the last neutrons. In particular, the pygmy dipole resonance was

suggested to influence the r-process nucleosynthesis [28], and efforts to include the exotic collective excitations has been pursued in the framework of the CN process models [19, 28–34]. However the assumption of the statistical compound states may not be appropriate in the case of small neutron separation energy. Effect of the weak neutron binding is partly taken into account in the direct capture models [35], which have however difficulty to include the collective correlations.

The purpose of our study is to formulate a microscopic model of radiative neutron capture reaction which is relevant to the r-process. Namely we intend to take into account the various nuclear structure effects, which are not included in the conventional direct capture models. We intend also to describe the whole process of (n, γ) reaction on a single quantum many-body theory so that we can avoid the statistical assumption of the CN process. To this end we adopt the continuum random-phase approximation (cRPA) [36–38], which is formulated as a linear response theory based on the time-dependent density functional theory (TDDFT) [39]. In a previous publication [40], we have reported a prototype formulation which describes the radiative capture process $(A - 1) + n \rightarrow A^* \rightarrow A_{\text{g.s.}} + \gamma$, i.e. a gamma-transition from continuum excited states A^* , which couples to the neutron scattering state $(A - 1) + n$, to the ground state $A_{\text{g.s.}}$ of the residual nucleus A . This formulation enables us to describe the collective excitations such as the pygmy and/or giant resonances, or the RPA correlation in general in the continuum excited states A^* . Note however that the final states of the actual (n, γ) reaction are not only the ground state $A_{\text{g.s.}}$ but also low-lying excited states A^{**} . Therefore, in the present paper, we extend the formalism so that it can describe the latter case, i.e. the (n, γ) reaction $(A - 1) + n \rightarrow A^* \rightarrow A^{**} + \gamma$ populating the low-lying excited states A^{**} . This is a necessary extension to evaluate the total neutron capture cross section to which gamma-decays to excited states contribute. Furthermore we will take into account correlations in the low-lying excited states A^{**} , such as surface vibrational modes.

One of the keys of the extension is given in a preceding paper [41], where we have formulated an extended linear response theory (the continuum random-phase approximation) to describe photo-absorption transitions $A^{**} + \gamma \rightarrow A^*$ from a low-lying excited state A^{**} to the continuum excited states A^* . On the basis of this achievement, we formulate in the present paper a framework to calculate the (n, γ) cross section. An important key for this purpose is the method of Zangwill and Soven [42], which enables us to define the T matrix for photo-absorption followed by particle-emission. Combining these key formalisms, we

describe partial cross sections of (γ, n) reaction $A^{**} + \gamma \rightarrow A^* \rightarrow n + (A - 1)$ for individual channels of the neutron emission $A^* \rightarrow n + (A - 1)$. We then obtain the (n, γ) cross section for the inverse process $(A - 1) + n \rightarrow A^* \rightarrow A^{**} + \gamma$, using the reciprocity theorem. Details of the formulation is given in Sec. II.

We demonstrate in Sec. III new features of the present theory by performing a numerical calculation for radiative neutron capture on ^{139}Sn with E1 and E2 transitions populating low-lying quadrupole and octupole states as well as the ground state in ^{140}Sn . We will show that the presence of the low-lying octupole state brings new aspects in the (n, γ) reactions originating from strong collectivity of this state. We shall discuss also that the present cRPA approach describes different kinds of resonance structure emerging in the capture reaction, including narrow resonances originating from non-collective states as well as the giant resonances and the single-particle resonances. We draw conclusions in Sec. IV.

II. THEORY

In this section we formulate a scheme to describe a radiative neutron capture reaction $(A - 1) + n \rightarrow A^* \rightarrow A^{**} + \gamma$ where the final state of the gamma-transition is a low-lying excited state A^{**} . We first describe photo-absorption reaction $A^{**} + \gamma \rightarrow A^*$ assuming that both initial and final states are described by the continuum random-phase approximation (cRPA) to the time-dependent density functional theory (TDDFT) (subsections II A and II B). In case the excited state A^* is located above the neutron separation energy, A^* decays by emitting a neutron $A^* \rightarrow (A - 1) + n$. In the framework of the continuum random-phase approximation the configuration of the daughter nucleus $(A - 1)$ is a one-hole state with respect to the ground state of A . It is then possible to derive partial photo-absorption cross sections for individual channels of the scattering states $(A - 1) + n$ by using the Zangwill and Soven method (subsection II C). Finally we obtain the neutron capture cross section for the inverse process $(A - 1) + n \rightarrow A^* \rightarrow A^{**} + \gamma$ using the detailed balance (subsection II D).

A. The photo-absorption cross section between RPA excited states

We express an initial state A^{**} of photo-absorption reaction as $|iL_iM_i\rangle$ with excitation energy E_i , where L_iM_i are the angular momentum numbers. We also express an excited

state A^* as $|kLM(E)\rangle$ with the angular quantum numbers LM . The excitation energy E is shown explicitly as A^* is a state in the continuum spectrum. k represents other quantum numbers. Normalization is $\langle k'L'M'(E')|kLM(E)\rangle = \delta_{k'L'M',kLM}\delta(E - E')$.

The photoabsorption cross section of the transition from $|iL_iM_i\rangle$ to states with angular momentum L and energy $E = E_i + E_\gamma$ is given generally by [43–45]

$$\sigma_{iL_i+\gamma\rightarrow L}^\lambda(E_\gamma) = f_\lambda(E_\gamma) \sum_k B(M_\lambda, iL_i \rightarrow kL(E)) = \frac{f_\lambda(E_\gamma)}{2L_i + 1} S(M_\lambda; iL_i, L; E) \quad (1)$$

for electromagnetic multipole $\hat{M}_{\lambda\mu}$ transition with photon energy E_γ in terms of the reduced matrix element

$$B(M_\lambda, iL_i \rightarrow kL(E)) = \frac{1}{2L_i + 1} |\langle kL(E) | \hat{M}_\lambda | iL_i \rangle|^2, \quad (2)$$

or the strength function

$$\begin{aligned} S(M_\lambda; iL_i, L; E) &= \sum_{kMM_i\mu} |\langle kLM(E) | \hat{M}_{\lambda\mu} | iL_iM_i \rangle|^2 \\ &= \sum_k |\langle kL(E) | \hat{M}_\lambda | iL_i \rangle|^2, \end{aligned} \quad (3)$$

and a kinematical factor

$$f_\lambda(E_\gamma) = \frac{(2\pi)^3(\lambda + 1)e^2}{\lambda[(2\lambda + 1)!!]^2} \left(\frac{E_\gamma}{\hbar c}\right)^{2\lambda-1}. \quad (4)$$

We assume that both excited states $|iL_iM_i\rangle$ and $|kLM(E)\rangle$ are those which can be described by cRPA based on the TDDFT. In other words, the model space is spanned by all the particle-hole configurations including scattering single-particle states. In the present work we assume that a nucleus A has closed-shell configurations (or sub-shell-closed configurations) for both neutrons and protons where the pair correlation can be neglected. Inclusion of the pairing is feasible with use of the method in Ref.[40], but we leave it for future publications.

As shown in Ref.[41], the strength function $S(M_\lambda; iL_i, L; E)$ for transitions from an excited state iL_i is rewritten as another strength function

$$S(F_L; g, L; E) \equiv \sum_k |\langle kL(E) | \hat{F}_L | 0_g^+ \rangle|^2 = S(M_\lambda; iL_i, L; E) \quad (5)$$

for an operator

$$\hat{F}_{LM} \equiv \sum_{\mu M_i} \langle \lambda\mu L_i M_i | LM \rangle [\hat{M}_{\lambda\mu}, \hat{O}_{iL_iM_i}^\dagger], \quad (6)$$

defined by a commutator between $\hat{M}_{\lambda\mu}$ and the RPA creation operator $\hat{O}_{iL_iM_i}^\dagger$ of the low-lying excited state $|iL_iM_i\rangle = \hat{O}_{iL_iM_i}^\dagger |0_g^+\rangle$. Note that the matrix elements in the strength function $S(F_L; g, L; E)$ are those between the ground state $|0_g^+\rangle$ and the RPA excited states $|kLM(E)\rangle$ for the operator \hat{F}_{LM} . Since the operator \hat{F}_{LM} is a one-body, though non-local, operator, it is possible to calculate the strength function $S(F_L; g, L; E)$ using an extended linear response formulation of the cRPA[41].

B. Linear response formalism

Here we recapitulate briefly an essence of the formulation[41] by omitting the angular momentum algebra.

The non-local one-body operator $\hat{F} = [\hat{M}, \hat{O}_i^\dagger]$ is expressed as

$$\hat{F} = \iint dx dy F(x, y) \psi^\dagger(x) \psi(y), \quad (7)$$

where $\psi^\dagger(x)$ and $\psi(y)$ are the creation and annihilation operators of the nucleon, and $F(x, y)$ is the coordinate representation of the matrix element. Here x (and y) is shorthand notation of the space coordinate \vec{r} and the spin variable $\sigma = \uparrow, \downarrow$, i.e. $x = \vec{r}\sigma$, $\int dx = \sum_\sigma \int d\vec{r}$. Using the linear response $\delta\rho(x, y, \omega)$ of density matrix $\rho(x, y) = \langle \hat{\rho}(x, y) \rangle$, $\hat{\rho}(x, y) = \psi^\dagger(y) \psi(x)$ for the perturbation \hat{F} , we can calculate the strength function $S(F; \hbar\omega) = \sum_k |\langle k(E) | \hat{F} | 0 \rangle|^2$ ($E = \hbar\omega$) as

$$S(F; \hbar\omega) = -\frac{1}{\pi} \text{Im} \iint dx dy F^*(x, y) \delta\rho(x, y, \omega). \quad (8)$$

In TDDFT scheme the density matrix response $\delta\rho(x, y, \omega)$ obeys the linear response equation

$$\delta\rho(x, y, \omega) = \iint dx' dy' R_0(x, y; y', x'; \omega) (F(x', y') + v_{\text{ind}}(x', \omega) \delta(x' - y')). \quad (9)$$

Here $v_{\text{ind}}(x, \omega)$ is a time-dependent part of the Hartree-Fock (or Kohn-Sham) potential originating from the density response, which is called the induced field. Assuming that the HF (KS) mean-field $U[\rho](x)$ is local, it is given by

$$v_{\text{ind}}(x, \omega) = \frac{\delta U(x)}{\delta \rho} \delta\rho(x, \omega) \quad (10)$$

with $\delta\rho(x, \omega) \equiv \delta\rho(x, x, \omega)$. The function R_0 is an unperturbed response function for the density matrix, and given by

$$R_0(x, y; y', x'; \omega) \equiv \sum_{ph} \left\{ \frac{\langle 0 | \hat{\rho}(x, y) | ph \rangle \langle ph | \hat{\rho}(y', x') | 0 \rangle}{\hbar\omega - (\epsilon_p - \epsilon_h) + i\eta} - \frac{\langle 0 | \hat{\rho}(y', x') | ph \rangle \langle ph | \hat{\rho}(x, y) | 0 \rangle}{\hbar\omega + (\epsilon_p - \epsilon_h) + i\eta} \right\} \quad (11)$$

in the spectral representation in terms of the single-particle eigenstates in the static HF (KS) potential $U[\rho_0](x)$. $|ph\rangle = a_p^\dagger a_h |0\rangle$ is one-particle-one-hole configuration, ϵ_p and ϵ_h are single-particle energies of the particle and hole orbits. η is a positive infinitesimal constant.

The response function R_0 is expressed also as

$$R_0(x, y; y', x'; \omega) = \sum_h \left\{ \phi_h^*(y) G_0(x, x', \epsilon_h + \hbar\omega + i\eta) \phi_h(y') + \phi_h^*(x') G_0(y', y, \epsilon_h - \hbar\omega - i\eta) \phi_h(x) \right\}, \quad (12)$$

where $G_0(x, x', \epsilon)$ is the single-particle Green's function for the static HF (KS) potential U_0 , and $\phi_h(x)$ is the wave function of the hole orbit h . The Green's function satisfies a proper asymptotic boundary condition for $|x|, |x'| \rightarrow \infty$ so that it describes scattering waves for unbound orbits.

We refer the readers to Ref.[41] for equations with the angular momentum algebra.

C. The Zangwill-Soven method for partial photo-absorption cross section

In the linear response formalism discussed above, unbound particle states p represent the scattering states. It is therefore possible to describe decay of the RPA excited states with emission of a neutron (or a proton). Following Zangwill and Soven [42], we shall calculate partial (γ, n) cross section for individual decay channels.

We first note that the strength function Eq. (5) is rewritten as

$$\begin{aligned} S(\hat{F}; \hbar\omega) &= -\frac{1}{\pi} \text{Im} \iiint dx dy dx' dy' v_{\text{scf}}^*(x, y, \omega) R_0(x, y; y', x'; \omega) v_{\text{scf}}(x', y', \omega) \\ &= \sum_{ph} \left| \langle ph | \hat{V}_{\text{scf}}(\hat{F}; \omega) | 0 \rangle \right|^2 \delta(\hbar\omega - (\epsilon_p - \epsilon_h)). \end{aligned} \quad (13)$$

Here $\hat{V}_{\text{scf}}(\hat{F}; \omega)$ is a one-body field, called the self-consistent field [42, 46], defined as a sum

of induced field \hat{V}_{ind} and the perturbing field \hat{F} :

$$\hat{V}_{\text{sfc}}(\hat{F}; \omega) \equiv \hat{F} + \hat{V}_{\text{ind}}(\hat{F}; \omega) = \iint dx dy v_{\text{sfc}}(x, y, \omega) \hat{\rho}(y, x), \quad (14)$$

$$v_{\text{sfc}}(x, y, \omega) \equiv F(x, y) + \frac{\delta U(x)}{\delta \rho} \delta \rho(x, \omega) \delta(x - y). \quad (15)$$

Note that matrix element $\langle ph | \hat{V}_{\text{sfc}}(\hat{F}; \omega) | 0 \rangle$ is a T matrix for the (γ, n) reaction under consideration. This is seen in

$$\langle ph | \hat{V}_{\text{sfc}}(\hat{F}; \omega) | 0 \rangle = \langle ph | \hat{F} | 0 \rangle + \int dx \langle ph | \frac{\delta U(x)}{\delta \rho} \hat{\rho}(x) | 0 \rangle \delta \rho(x, \omega). \quad (16)$$

The first term $\langle ph | \hat{F} | 0 \rangle$ corresponds to the diagram representation shown in Fig. 1(a). The density response $\delta \rho(x, \omega)$ in the second term can be expanded in infinite series

$$\delta \rho = R_0 F + R_0 \frac{\delta U}{\delta \rho} \delta \rho = R_0 F + R_0 \frac{\delta U}{\delta \rho} R_0 F + R_0 \frac{\delta U}{\delta \rho} R_0 \frac{\delta U}{\delta \rho} R_0 F + \dots, \quad (17)$$

representing symbolically the linear response equation (9). We notice that this infinite series correspond to ring diagrams, and the matrix element $\langle ph | \hat{V}_{\text{sfc}}(\hat{F}; \omega) | 0 \rangle$ is represented by the diagrams shown in Fig. 1.

These diagrams indicate that the matrix element $\langle ph | \hat{V}_{\text{sfc}}(\hat{F}; \omega) | 0 \rangle$ represents the transition amplitude for the electromagnetic operator \hat{M} between the low-lying excited state $|i\rangle$ and a RPA excited state (represented by series of the ring diagrams) which is connected to a specific particle-hole configuration $|ph\rangle$. In the case when the particle state p is an unbound single-particle state, it represents the transition-matrix, T matrix, of the (γ, n) reaction where the final state consists of a unbound neutron (specified by the particle configuration p) and the residual nucleus $(A - 1)$ with one-hole configuration $a_h |0\rangle$. We call it the RPA T matrix. We give more detailed discussion in Appendix A.

Consequently each term in the r.h.s. of Eq. (13) is related to the partial photoabsorption cross section for a (γ, n) process, A (state i) $+ \gamma \rightarrow (A - 1)$ (one-hole state $a_h |0\rangle$) $+ n$ (single-particle state p):

$$\sigma_{i+\gamma \rightarrow ph}^\lambda(E_\gamma) = f_\lambda(E_\gamma) \left| \langle ph | \hat{V}_{\text{sfc}}(\hat{F}; \omega) | 0 \rangle \right|^2 \delta(\hbar\omega - (\epsilon_p - \epsilon_h)). \quad (18)$$

with $E_\gamma = \hbar\omega - E_i$.

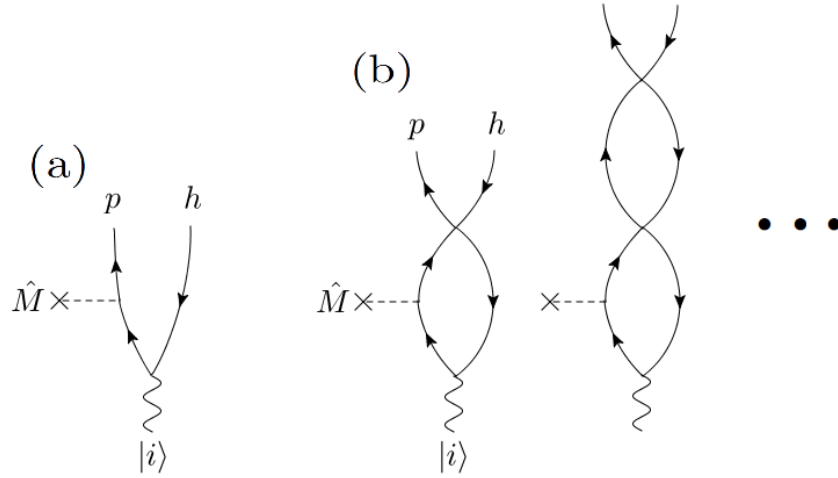


FIG. 1. The diagrams representing the matrix element $\langle ph | \hat{V}_{\text{scf}}(\hat{F}; \omega) | 0 \rangle$. (a) and (b) correspond to the first and second terms of r.h.s. of Eq.(16), respectively. Note that the electromagnetic operator \hat{M} acts also on the hole line.

The photo-absorption cross section can be written also in terms of the single-particle Green's function. Inserting Eq.(12) to Eq.(13), we have the partial photo-absorption cross section:

$$\sum_{p(\epsilon_p=\epsilon)} \sigma_{i+\gamma \rightarrow ph}^\lambda(E_\gamma) = -\frac{f_\lambda(E_\gamma)}{\pi} \text{Im} \iiint dx dy dx' dy' \phi_h^*(y) v_{\text{scf}}^*(x, y, \omega) \times G_{0c}(x, x', \hbar\omega + \epsilon_h + i\eta) v_{\text{scf}}(x', y', \omega) \phi_h(y'), \quad (19)$$

for final states consisting of an escaping neutron with energy $\epsilon = \hbar\omega + \epsilon_h = E_\gamma + E_i + \epsilon_h$ and a one-hole state $a_h |0\rangle$ of the residual nucleus $(A-1)$. Here G_{0c} is the single-particle Green's function in which a contribution of bound orbits is removed:

$$G_{0c}(x, x', \epsilon) \equiv G_0(x, x', \epsilon) - \sum_{i(\epsilon_i < 0)} \frac{\phi_i(x) \phi_i^*(x')}{\epsilon - \epsilon_i}. \quad (20)$$

D. Concrete expressions for (γ, n) and (n, γ) cross sections

In actual application we consider the angular momentum algebra with the polar-coordinate representation. For example $v_{\text{scf}}(x, y, \omega)$ is represented as

$$v_{LM}^{\text{scf}}(x, y, \omega) = \sum_{ljm, l'j'm'} Y_{l'j'm'}(\hat{x}) \frac{1}{\sqrt{2j'+1}} \langle jmLM | j'm' \rangle \frac{v_{L,l'j',lj}^{\text{scf}}(r_x, r_y)}{r_x r_y} Y_{ljm}^*(\hat{y}). \quad (21)$$

Here Y_{ljm} is the spin spherical harmonics. We specify the escaping neutron with energy ϵ and the partial wave quantum numbers lj , and express the final state $|ph\rangle$ as $|\langle [l_p j_p, n_h l_h j_h]_{LM} \rangle = \sum_{m_p m_h} \langle j_p m_p j_h m_h | LM \rangle a_{\epsilon l_p j_p m_p}^\dagger a_{n_h l_h j_h m_h} |0\rangle$ with L being the total angular momentum, which is identical to that of the RPA excited state A^* . Accordingly we obtain the expression for the partial photo-absorption cross section for the specific channel of neutron decay as

$$\begin{aligned} \sigma_{iL_i+\gamma\rightarrow[\epsilon l_p j_p h]_L}^\lambda(E_\gamma) &= f_\lambda(E_\gamma) \frac{1}{2L_i+1} \left| \langle [l_p j_p h]_L | \hat{V}_{\text{scf}}(\hat{F}_L; \omega) | 0 \rangle \right|^2 \\ &= -\frac{f_\lambda(E_\gamma)}{\pi(2L_i+1)} \\ &\quad \times \text{Im} \iiint \int dr_x dr_y dr_{x'} dr_{y'} \phi_{n_h l_h j_h}^*(r_y) v_{L, l_p j_p, l_h j_h}^{\text{scf}*}(r_x, r_y, \omega) \\ &\quad \times G_{0c, l_p j_p}(r_x, r_{x'}, \epsilon_h + \hbar\omega + i\eta) v_{L, l_p j_p, l_h j_h}^{\text{scf}}(r_{x'}, r_{y'}, \omega) \phi_{n_h l_h j_h}(r_{y'}). \quad (22) \end{aligned}$$

Note that $\hbar\omega = E_\gamma + E_i$ is the excitation energy of the state A^* of the nucleus A . Expression of $v_{L, l_p j_p, l_h j_h}^{\text{scf}}(r_{x'}, r_{y'}, \omega)$ and a closed form expression of the cross section are given in Appendix B.

Finally, we use the detailed balance to obtain the radiative neutron capture cross section for the reaction $(A-1) + n \rightarrow A^* \rightarrow A^{**} + \gamma$:

$$\sigma_{[\epsilon l_p j_p h]_L \rightarrow iL_i + \gamma}^\lambda(\epsilon) = \frac{2L_i+1}{2j_h+1} \frac{E_\gamma^2}{2mc^2\epsilon} \sigma_{iL_i+\gamma\rightarrow[\epsilon l_p j_p h]_L}^\lambda(E_\gamma). \quad (23)$$

for an incident neutron with partial wave $l_p j_p$ and energy ϵ impinging on the $(A-1)$ nucleus with a one-hole configuration h , and gamma transition to the excited state $|iL_i M_i\rangle$. The total cross section is obtained by summing all the contributions of the partial waves $l_p j_p$ and the total angular momentum L of the system.

III. NUMERICAL EXAMPLES

A. Setting

We shall apply the theory to radiative neutron capture reaction on a neutron-rich nucleus ^{139}Sn , which populates the ground and low-lying excited states of ^{140}Sn after gamma transition. We have chosen these isotopes since the neutron separation energy of ^{140}Sn is estimated to be ~ 3 MeV [47] and these isotopes are relevant to the r-process. Another

reason is that ^{140}Sn has a subshell closure at the $2f_{7/2}$ orbit for neutrons, and the pairing correlation neglected in the present formulation is expected to be weak.

Numerical calculations are performed with the same setting as in our previous paper [41]. We use a Woods-Saxon potential in place of the static self-consistent field U_0 and a Skyrme-type contact interaction as the residual two-body force, given by

$$v_{ph}(\mathbf{r}, \mathbf{r}') = \left\{ t_0(1 + x_0 P_\sigma) + \frac{t_3}{12}(1 + x_3 P_\sigma)\rho(r) \right\} \delta(\mathbf{r} - \mathbf{r}'). \quad (24)$$

The details including the parameters are the same as those in [41]. We describe the single-particle wave function by solving the radial Schrödinger equation with the Runge-Kutta method up to a maximal radius $R_{\text{max}} = 20$ fm (with interval $\Delta r = 0.2$ fm). At $r = R_{\text{max}}$ the single-particle wave function is connected to the asymptotic wave, i.e. the Hankel function with an appropriate (complex) wave number. The small real constant η in the response equation is set to $\eta = 1.0 \times 10^{-5}$ or 0.1 MeV.

In the present analysis, we intend to demonstrate effects of the RPA correlations on the (n, γ) reaction, in particular, roles of the collectivity which may exist both in the scattering state of $^{139}\text{Sn} + n$ and the final states of ^{140}Sn . We focus on the low-lying quadrupole and octupole vibrational states as well as the dipole and quadrupole giant resonances. Other types of the particle-hole excitations such as the soft dipole mode and non-collective excitations are also discussed. We take into account the RPA correlation for the states with natural spin-parity $L^\pi = 1^-, 2^+$ and 3^- whereas we neglect it for other spin-parities.

Table I shows the Woods-Saxon single-particle orbits. The highest occupied neutron orbit in ^{140}Sn is $2f_{7/2}$ with $\epsilon_{2f_{7/2}} = -2.59$ MeV (the Fermi energy). The configuration of the ground state of ^{139}Sn is assumed to be a configuration with neutron one-hole in $2f_{7/2}$ with spin-parity $j_h^\pi = 7/2^-$. We denote it $^{139}\text{Sn}(7/2^-)$ in the following. The RPA calculation for ^{140}Sn brings about several bound excited states below the neutron separation energy $S_{1n} = 2.59$ MeV (see Fig. 2 of Ref. [41]). Among them we adopt the lowest-lying excited states, i.e. $2_{1,2}^+$ and 3_1^- states, as the final states $|iL_i\rangle$ of the $^{139}\text{Sn}(n, \gamma)^{140}\text{Sn}$ reaction. The excitation energy of these states are $E_{2_1^+} = 0.888$ MeV, $E_{2_2^+} = 1.093$ MeV, $E_{3_1^-} = 1.768$ MeV. As seen in the RPA forward amplitudes X_{ph} of these states (Tables II and III), the 3_1^- state exhibits a moderately strong collectivity, i.e. it contains many particle-hole configurations both in neutrons and protons, typical of the surface vibrational octupole state. The 2_1^+ and 2_2^+ states consist mostly of two neutron particle-hole configurations, $(1h_{9/2})(2f_{7/2})^{-1}$ and

TABLE I. Single-particle energies of the adopted Woods-Saxon potential for ^{140}Sn . Several orbits around the Fermi energy (indicated by lines) are listed.

neutron ϵ [MeV]		proton ϵ [MeV]	
$2f_{5/2}$	-0.31	$1h_{11/2}$	-11.40
$3p_{1/2}$	-0.81	$2d_{3/2}$	-11.61
$3p_{3/2}$	-1.46	$2d_{5/2}$	-14.06
$1h_{9/2}$	-1.53	$1g_{7/2}$	-15.08
$2f_{7/2}$	-2.59	$1g_{9/2}$	-19.97
$1h_{11/2}$	-6.64	$2p_{1/2}$	-21.75
$3s_{1/2}$	-8.65	$2p_{3/2}$	-23.02
$2d_{3/2}$	-8.65	$1f_{5/2}$	-24.81
$2d_{5/2}$	-10.40		
$1g_{7/2}$	-10.96		
$1g_{9/2}$	-14.64		

$(3p_{3/2})(2f_{7/2})^{-1}$ while the correlation causes strong mixing among them.

For the gamma transition, we mostly discuss the E1 transition, but we also mention briefly the E2 case. We take into account all possible angular and spin quantum numbers of the total system (both for the scattering state of $^{139}\text{Sn} + n$ and the final states of ^{140}Sn) as long as they are allowed by the angular momentum coupling of the adopted final states ($L_i^\pi = 0_{\text{g.s.}}^+, 2_{1,2}^+$ and 3_1^-) and the multipolarity ($\lambda = 1, 2$) of the gamma ray. Namely, we describe $^{139}\text{Sn}(7/2^-) + n \rightarrow ^{140}\text{Sn}(1^-) \rightarrow ^{140}\text{Sn}(\text{g.s.}) + \gamma$, $^{139}\text{Sn}(7/2^-) + n \rightarrow ^{140}\text{Sn}(1^-, 2^-, 3^-) \rightarrow ^{140}\text{Sn}(2_{1,2}^+) + \gamma$, $^{139}\text{Sn}(7/2^-) + n \rightarrow ^{140}\text{Sn}(2^+, 3^+, 4^+) \rightarrow ^{140}\text{Sn}(3_1^-) + \gamma$ for the E1 transition while $^{139}\text{Sn}(7/2^-) + n \rightarrow ^{140}\text{Sn}(2^+) \rightarrow ^{140}\text{Sn}(\text{g.s.}) + \gamma$, $^{139}\text{Sn}(7/2^-) + n \rightarrow ^{140}\text{Sn}(0^+, 1^+, 2^+, 3^+, 4^+) \rightarrow ^{140}\text{Sn}(2_{1,2}^+) + \gamma$, $^{139}\text{Sn}(7/2^-) + n \rightarrow ^{140}\text{Sn}(1^-, 2^-, 3^-, 4^-, 5^-) \rightarrow ^{140}\text{Sn}(3_1^-) + \gamma$. for the E2 case. We include all the partial waves of the incident neutron which are allowed by the coupling to the the spin-parity $7/2^-$ of the target nucleus ^{139}Sn . Its maximum is $l_p, j_p = 8, 17/2$.

TABLE II. The RPA forward amplitudes X_{ph} of the 2_1^+ and 2_2^+ state. Particle-hole configurations with large amplitude $|X_{ph}| > 0.1$ are listed. The RPA backward and forward amplitudes X_{ph} and Y_{ph} are calculated using a method of Ref.[48].

neutron config.	$X_{ph}^{2_1^+}$	$X_{ph}^{2_2^+}$
$(1h_{9/2})(2f_{7/2})^{-1}$	-0.601	0.791
$(3p_{3/2})(2f_{7/2})^{-1}$	0.789	0.600

TABLE III. The RPA forward amplitudes X_{ph} of the 3_1^- state. Particle-hole configurations with large amplitude $|X_{ph}| > 0.1$ are listed. The neutron single-particle orbit $1i_{13/2}$ is a resonance in the continuum.

neutron config.	$X_{ph}^{3_1^-}$	proton config.	$X_{ph}^{3_1^-}$
$(1i_{13/2})(2f_{7/2})^{-1}$	0.831	$(1h_{11/2})(1g_{9/2})^{-1}$	-0.285
$(1i_{13/2})(1h_{11/2})^{-1}$	0.354	$(1g_{7/2})(2p_{1/2})^{-1}$	0.203
$(1h_{9/2})(2d_{3/2})^{-1}$	-0.299	$(2d_{5/2})(2p_{1/2})^{-1}$	0.176
$(1h_{9/2})(1g_{7/2})^{-1}$	-0.189	$(2d_{5/2})(2p_{3/2})^{-1}$	0.135
$(2f_{5/2})(3s_{1/2})^{-1}$	0.134	$(1j_{15/2})(1g_{9/2})^{-1}$	0.129
$(2g_{9/2})(2f_{7/2})^{-1}$	0.133	$(2f_{7/2})(1g_{9/2})^{-1}$	-0.129
$(2f_{5/2})(2d_{3/2})^{-1}$	-0.126	$(2d_{3/2})(2p_{3/2})^{-1}$	-0.120
$(3p_{3/2})(2d_{3/2})^{-1}$	-0.112	$(3p_{3/2})(1g_{9/2})^{-1}$	-0.103
$(2j_{15/2})(1g_{9/2})^{-1}$	0.108	$(1g_{7/2})(1f_{5/2})^{-1}$	0.102
$(2f_{5/2})(1g_{7/2})^{-1}$	-0.101		

B. Low energy (n, γ) cross section with E1 transition

Figure 2 shows the cross sections of neutron capture with E1 for low neutron kinetic energy relevant to the r-process, calculated separately for each final state. A characteristic feature is that the cross sections exhibit significant differences for different final states. In particular most dominant transition at low energy is the ones to the 2_1^+ and 2_2^+ states rather than to the ground state. Another noticeable feature is that the transition to the octupole

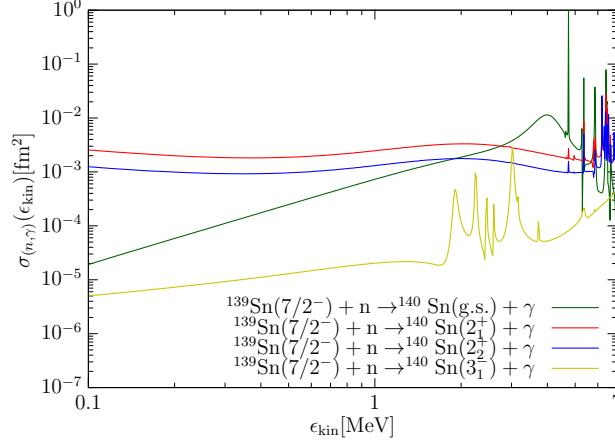


FIG. 2. The calculated (n, γ) cross sections for $^{139}\text{Sn}(7/2^-) + n \rightarrow ^{140}\text{Sn} + \gamma$ with E1 transitions populating different low-lying states in ^{140}Sn ; the ground state (plotted with a green curve), the low-lying 2_1^+ and 2_2^+ states (red and blue curves respectively), and the octupole vibrational state 3_1^- (yellow curve). The horizontal axis is kinetic energy ϵ_{kin} of the incident neutron. The smoothing parameter is $\eta = 10^{-5}$ MeV.

vibrational state 3_1^- is present although the absolute magnitude is small. It is noted that there is no negative parity one-particle one-hole ($1p1h$) configuration with energy smaller the neutron separation energy 2.59 MeV. The collective 3_1^- is exceptional as this state emerges at low energy due to the RPA correlation. The third observation is that the cross sections exhibit many resonance-like behaviors above 2 MeV whereas they are smooth below 2 MeV. In the following we shall discuss these features in more details.

1. Transitions to the ground state

Let us discuss the (n, γ) reaction where the gamma transition populates directly the ground state of ^{140}Sn , whose cross section is the green curve in Fig. 2. In order to analyze the structures seen in Fig. 2, we decompose the cross section with respect to the partial waves of the incident neutron. The decomposed cross sections are shown in Fig. 3. In the present case the relevant spin-parity of the total system $n + ^{139}\text{Sn}$ or that of excited continuum state of ^{140}Sn is 1^- . Thus the partial waves of the incident neutron are limited to $d_{5/2}$ and $g_{7/2,9/2}$ due to the angular momentum coupling to the ground state $^{139}\text{Sn}(7/2^-)$.

The cross section at low energy ≤ 1 MeV is dominated by the $d_{5/2}$ -wave since it has the lowest orbital angular momentum among the available partial waves. The s -wave capture

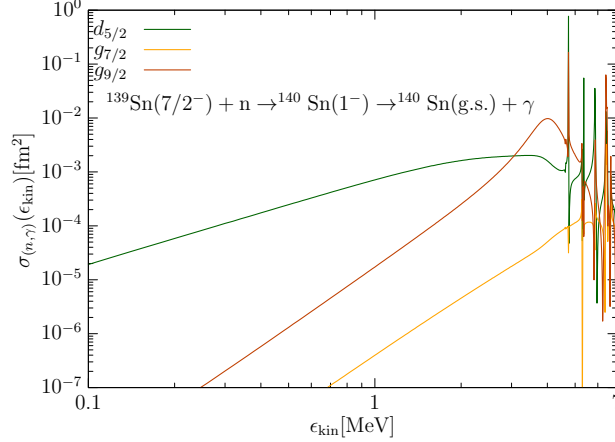


FIG. 3. The calculated partial (n, γ) cross sections for $^{139}\text{Sn}(7/2^-) + n \rightarrow ^{140}\text{Sn}(1^-) \rightarrow ^{140}\text{Sn}(\text{g.s.}) + \gamma$ for E1 transitions, plotted separately for different partial waves of the incident neutron; $d_{5/2}$ (green curve), $g_{7/2}$ (orange), and $g_{9/2}$ (brown). The horizontal axis is the neutron kinetic energy ϵ_{kin} . The smoothing parameter is $\eta = 10^{-5}$ MeV.

is forbidden due to the angular coupling rule. The low energy behavior of the partial cross sections exhibits a scaling $\propto \epsilon^{l_p-1/2}$, which points to direct transitions from non-resonant partial waves to the ground state of ^{140}Sn . It is seen that a rather broad peak around $\epsilon_{\text{kin}} = 4$ MeV is that in the $g_{9/2}$ -wave. It is the E1 transition from the single-particle $g_{9/2}$ resonance to the bound $2f_{7/2}$ orbit which is vacant in ^{139}Sn . These features reflect the single-particle nature of the soft dipole excitation of ^{140}Sn .

Several sharp peaks in the energy range $\epsilon_{\text{kin}} > 4.5$ MeV are however cannot be of the single-particle origin. Indeed they originates from non-collective states whose main components are one-particle-one-hole ($1p1h$) configurations $\nu[(3p_{3/2})(3s_{1/2})^{-1}]$, $\nu[(3p_{1/2})(3s_{1/2})^{-1}]$, $\nu[(3p_{3/2})(2d_{3/2})^{-1}]$, $\nu[(3p_{1/2})(2d_{3/2})^{-1}]$, $\nu[(3p_{3/2})(2d_{5/2})^{-1}]$, and $\nu[(3p_{1/2})(2d_{5/2})^{-1}]$. Although the particle and hole orbits of these configurations are both bound orbits (see Table I), they couple to the scattering states of $n + ^{139}\text{Sn}$ via the residual interaction as is represented in Fig.4, and they form narrow resonances. Note that the non-collective states with proton $1p1h$ configurations also appear as narrow resonances.

In Fig. 5 we magnify the resonance structures in the range of $\epsilon_{\text{kin}} = 5 - 7$ MeV. We see clearly interferences between the resonances and the non-resonant capture. Note that dominant partial wave contributing to the peak as well as the interference pattern are quite different for different resonances, reflecting the non-collective nature of these resonance states.

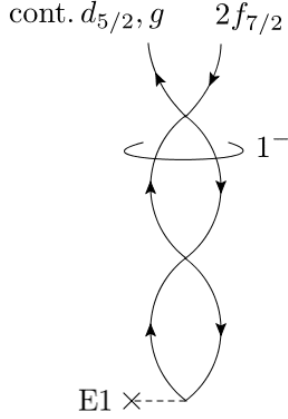


FIG. 4. The diagrams representing (n, γ) reaction of $^{139}\text{Sn}(7/2^-) + n \rightarrow ^{140}\text{Sn}(1^-) \rightarrow ^{140}\text{Sn}(\text{g.s.}) + \gamma$.

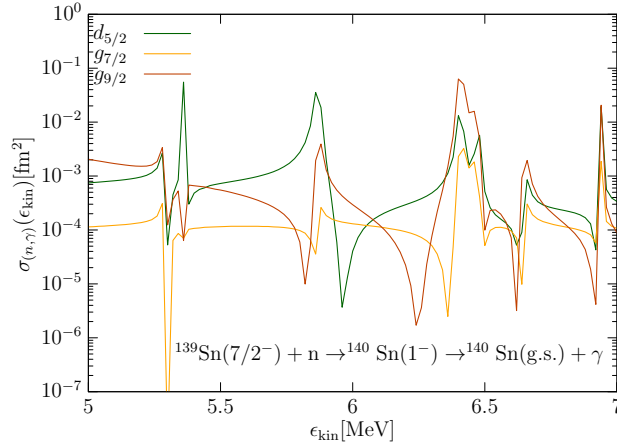


FIG. 5. The same as Fig. 3, but a magnification in the range of $\epsilon_{\text{kin}} = 5.0 - 7.0$ MeV.

2. Transitions to the low-lying states $2_{1,2}^+$

The transitions decaying to the low-lying quadrupole states $2_{1,2}^+$ are most dominant at low energy as seen in Fig. 2. (red and blue curves). Here we shall discuss the one for 2_1^+ since the cross sections for 2_1^+ and 2_2^+ behave similarly.

The spin-parity of the total system relevant to the present case is $L^\pi = 1^-, 2^-$ and 3^- . Figure 6 shows the partial cross section decomposed with respect to the partial waves $l_p j_p$ of the incident neutron, plotted separately for $L^\pi = 3^-$ and 2^- in panels (a) and (b), respectively.

It is seen from comparison of Fig. 2 and Fig. 6 that a large cross section at low energy is attributed to the s -wave capture. A noticeable feature is that the s -wave capture is present

only for $L^\pi = 3^-$ but not for $L^\pi = 2^-$. Possible partial waves of incident neutron allowed for the total spin-parity $L^\pi = 3^-$ are s, d, g and i due to the the angular momentum coupling to spin $7/2^-$ of the target ^{139}Sn . However for $L^\pi = 2^-$ allowed partial waves are d, g and $i_{11/2}$ for $L^\pi = 2^-$, excluding the s -wave. This is the same reason why there is no s -wave capture in the transitions to the ground state. Consequently the transitions to $2_{1,2}^+$ dominate at low energy.

Another significant feature is that many resonance-like structures with narrow width are seen for $L^\pi = 3^-$, but not for $L^\pi = 2^-$, though the impact on the absolute cross section is small. Similarly to the transition to the ground state (cf the previous subsection), the narrow resonances originate from the coupling between the non-resonant continuum states (s, d, g and i wave coupled to ^{139}Sn with $7/2^-$) and non-collective $1p1h$ configurations of both neutrons and protons, e.g. $\nu[(1h_{9/2})(3s_{1/2})^{-1}]$, $\nu[(2f_{5/2})(3s_{1/2})^{-1}]$, $\nu[(1h_{9/2})(2d_{3/2})^{-1}]$, $\nu[(3p_{3/2})(2d_{3/2})^{-1}]$, and $\nu[(2f_{5/2})(2d_{3/2})^{-1}]$ (cf. Fig. 7(a)). However, the spin-independent residual interaction Eq.(24) does not cause mixing among $1p1h$ states with unnatural spin-parity 2^- . In this case only the direct transition shown by the diagram Fig. 7(b) is relevant and the non-collective $1p1h$ states does not show up as resonances.

3. Transitions to the octupole vibrational state 3_1^-

Let us discuss the (n, γ) reaction whose final state is the octupole vibrational state 3_1^- at $E = 1.768$ MeV. The relevant spin-parity of the total system is $L^\pi = 2^+, 3^+$ and 4^+ , and we show in Fig. 8 partial (n, γ) cross sections for $L^\pi = 2^+$ and 3^+ separately. The low energy cross section $\epsilon_{\text{kin}} \leq 1$ MeV are dominated by the p -wave capture in both cases since $l = 1$ is the smallest orbital angular momentum of the neutron partial waves allowed both for $L^\pi = 2^+$ and 3^+ . Note that the capture in the p -wave (and other negative-parity partial waves) would not be present if the collective octupole state did not exist below the neutron separation energy.

The cross section for $L^\pi = 2^+$ (Fig. 8(a)) shows a significant enhancement around $\epsilon_{\text{kin}} \sim 2 - 3$ MeV with resonant structures. These resonance behaviors originate from excited 2^+ states of ^{140}Sn at $E = 4.8$ and 5.6 MeV, which appear as relatively large peaks in the E2 and isoscalar quadrupole strength functions shown in Fig. 2(b) of Ref. [41]. These quadrupole states have some collectivity, i.e. consisting of coherent neutron particle-hole

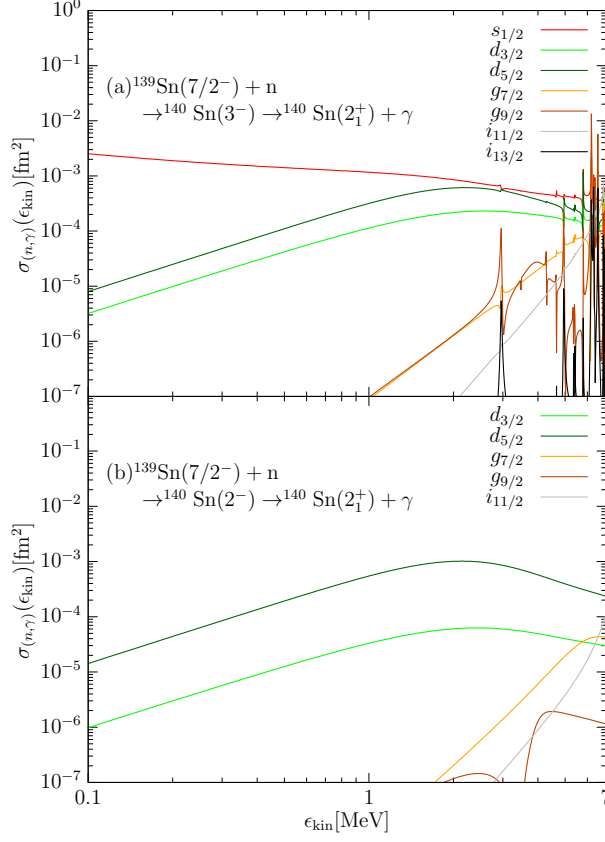


FIG. 6. The calculated partial (n, γ) cross sections for $^{139}\text{Sn}(7/2^-) + n \rightarrow ^{140}\text{Sn}(2^-, 3^-) \rightarrow ^{140}\text{Sn}(2_1^+) + \gamma$ for E1 transitions, plotted separately for different partial waves of the incident neutron; $s_{1/2}$ (red curve), $d_{3/2}$ (green), and $d_{5/2}$ (dark green) etc.. The panel (a) is for the total spin $L^\pi = 3^-$, and (b) for $L^\pi = 2^-$. The horizontal axis is the neutron kinetic energy ϵ_{kin} . The smoothing parameter is $\eta = 10^{-5}$ MeV.

admixture in addition to main proton particle-hole configurations $\pi[(1g_{9/2})(1g_{9/2})^{-1}]$, and $\pi[(2d_{5/2})(1g_{9/2})^{-1}]$. We remark that the collectivity in the quadrupole states is reflected in Fig. 8(a); the neutron partial waves $p_{3/2}$ and $f_{7/2,5/2}$ contribute coherently to the resonance structures. Such a coherence effect is not seen in the narrow resonance structures shown in Figs. 3, 5 and 6 where the relevant resonant states have a character of non-collective $1p1h$ excitations.

As for the case of $L^\pi = 3^+$ (Fig. 8(b)), the energy dependence is smooth without narrow resonance structures since there is no effect of the correlation, similarly to Fig. 6(b). The

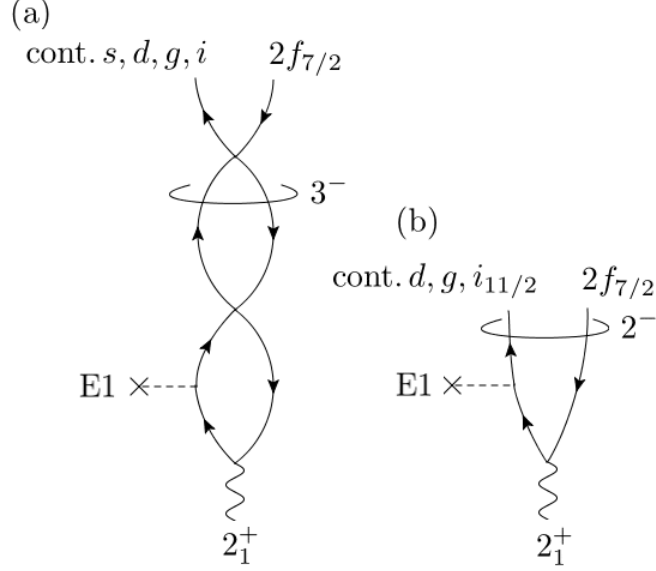


FIG. 7. The diagrams representing (n, γ) reaction of $^{139}\text{Sn}(7/2^-) + n \rightarrow ^{140}\text{Sn}(2^-, 3^-) \rightarrow ^{140}\text{Sn}(2_1^+) + \gamma$; (a) for the total spin $L^\pi = 3^-$ and (b) for $L^\pi = 2^-$.

process here is the direct capture represented by the diagram Fig. 9(b).

C. Cross section at higher energy

Let us examine a global behavior of the calculated cross sections in a wide energy region covering up to $\epsilon_{\text{kin}} \sim 20$ MeV although the result at high energies is not relevant to the r-process. We remark also that the model space of the present theory does not include multi-particle-multi-hole configurations, needed to describe the high level density and the complex structure of compound states at high excitation energy. In other words the present calculation lacks a part of the (n, γ) processes that is usually modeled in terms of the statistical treatment of the compound states.

Figure 10 shows the (n, γ) cross section for transitions to the low-lying $2_{1,2}^+$ and 3_1^- states as well as the ground state in ^{140}Sn . It is the same as Figure 2 but for $\epsilon_{\text{kin}} < 20$ MeV. The smoothing constant η is set to $\eta = 0.1$ MeV, which washes out narrow resonances.

We see several resonance-like peaks having sizable width at $\epsilon_{\text{kin}} \approx 4$ MeV, 8 MeV, 10 MeV and a bunch of peaks around $\epsilon_{\text{kin}} \approx 10 - 13$ MeV. The large peak at $\epsilon_{\text{kin}} \approx 4$ MeV is the one which we already discussed in subsection III B 1. It is essentially a single-particle resonance in the partial wave $g_{9/2}$, from which a single-particle E1 transition to the $2f_{7/2}$

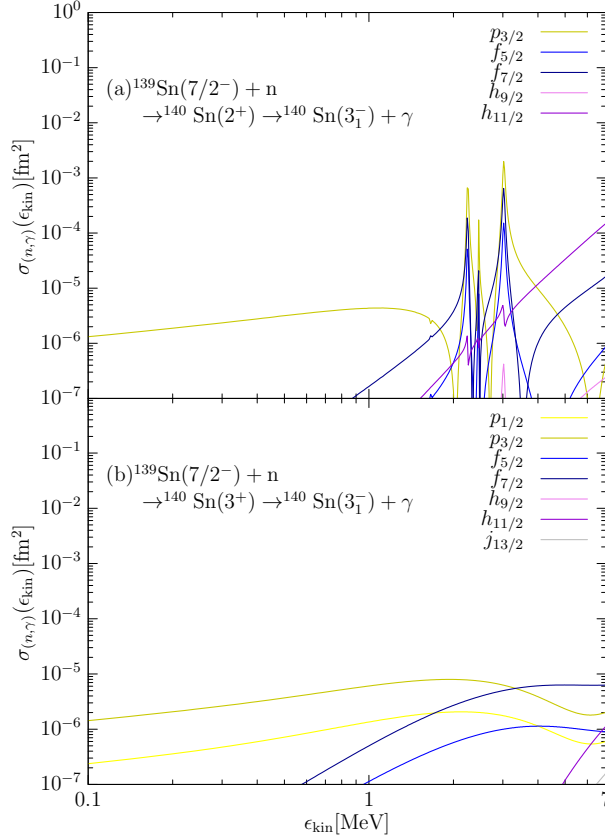


FIG. 8. The calculated partial (n, γ) cross sections for $^{139}\text{Sn}(7/2^-) + n \rightarrow ^{140}\text{Sn}(2^+, 3^+) \rightarrow ^{140}\text{Sn}(3_1^-) + \gamma$ for E1 transitions, plotted separately for different partial waves of the incident neutron; $p_{1/2}$ (yellow curve), $f_{5/2}$ (blue), and $h_{9/2}$ (pink) etc.. The panel (a) is for the total quantum number $L^\pi = 2^+$, and (b) for $L^\pi = 3^+$. The horizontal axis is the neutron kinetic energy ϵ_{kin} . The smoothing parameter is $\eta = 10^{-5}$ MeV.

orbit occurs.

The peak at $\epsilon_{\text{kin}} \approx 8$ MeV seen in the transition to the $2_{1,2}^+$ states reflects the single-particle $i_{11/2}$ resonance. Note that this peak is seen only for the transition to the $2_{1,2}^+$ states, but not to the ground state. The single-particle E1 transition is possible from the resonant i orbit to the bound $1h_{9/2}$ orbit (see Fig. 7(a)), which is occupied in the $2_{1,2}^+$ states as one of the main particle-hole configurations (see Table. II).

The largest peak at $\epsilon_{\text{kin}} \approx 10$ MeV is present in the transition to the octupole state 3_1^- . It originates from a single-particle resonance in the partial wave $j_{15/2}$. We remark that the

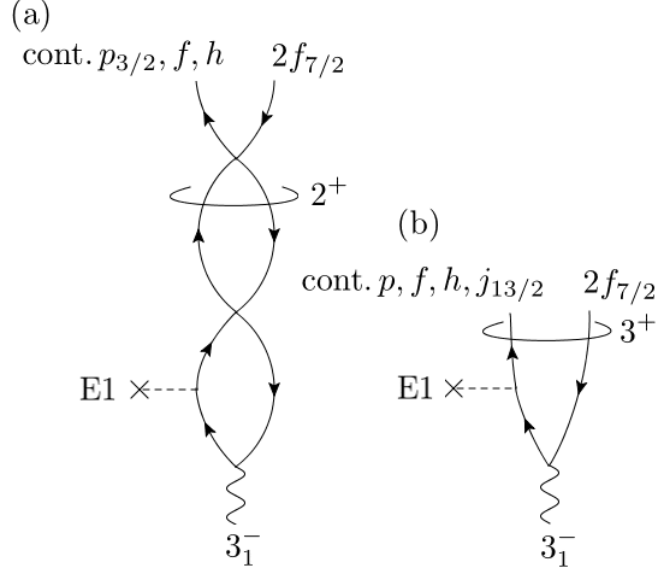


FIG. 9. The diagrams representing (n, γ) reaction of $^{139}\text{Sn}(7/2^-) + n \rightarrow ^{140}\text{Sn}(2^+, 3^+) \rightarrow ^{140}\text{Sn}(3_1^-) + \gamma$.

collectivity of the low-lying octupole state 3_1^- plays an essential role. The single-particle $j_{15/2}$ resonance has sizable E1 matrix element for a transition to the neutron $1i_{13/2}$ orbit, which is, however, unbound (resonance) in the present model. Therefore the capture is not possible via the single-particle process. In contrast, the 3_1^- state with the collective character of surface vibration can be a final state of the E1 transition from the neutron single-particle $j_{15/2}$ resonance since it contains configuration $(1i_{13/2})(2f_{7/2})^{-1}$ as one of main $1p1h$ components (cf. Table III).

A distribution of several peaks around $\epsilon_{\text{kin}} \approx 10 - 13$ MeV seen in the transition to the ground state (green curve) is another feature that points to importance of the collectivity in the (n, γ) reaction. These peaks are not related to the single-particle resonance, but they originate from the giant dipole resonance (GDR) in ^{140}Sn with spin-parity 1^- distributed around excitation energy $E \approx 12 - 16$ MeV. The capture proceeds through the GDR, which enhances gamma decay to the ground state.

D. (n, γ) reaction with E2 transition

We have calculated also the cross section for E2 transitions using the same formalism. The obtained cross sections are shown in Fig. 11 and 12 for the low energy part and the high

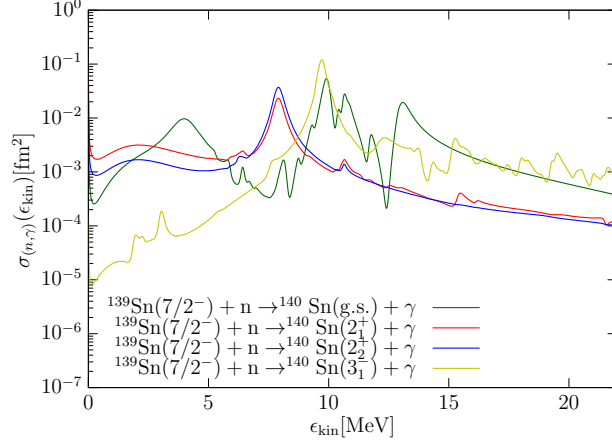


FIG. 10. The calculated (n, γ) cross sections for $^{139}\text{Sn}(7/2^-) + n \rightarrow ^{140}\text{Sn}$ with E1 transitions populating different low-lying states in ^{140}Sn ; the ground state (plotted with a green curve), the low-lying 2_1^+ and 2_2^+ states (red and blue curves respectively), and the octupole vibrational state 3_1^- (yellow curve). The horizontal axis is the neutron kinetic energy ϵ_{kin} . The smoothing parameter is $\eta = 0.1$ MeV.

energy part, respectively. The cross section for the E2 transition is smaller than those for E1 as is seen by comparing with the results for the E1 case (Figs. 2 and 10). An apparent reason is the kinematical factor which suppresses the high multipole transitions.

A noticeable difference from the E1 case is that the transitions to the ground state is dominant over other transitions feeding the low-lying excited states $2_{1,2}^+$ and 3_1^- . Here we note that the adopted E2 operator acts only on protons, neglecting the recoil correction of an order of A^{-1} . For this reason both the continuum excited state and the low-lying excited states need to include proton $1p1h$ configurations in order for the E2 transition to occur. Note that the calculated low-lying states in neutron-rich ^{140}Sn has dominant neutron character where the proton component is relatively small. This is especially the case for the 2^+ states (cf. Table II). Consequently, the transition to the low-lying $2_{1,2}^+$ and 3_1^- states are suppressed. For the transition to the ground state, on the contrary, the E2 transition occurs as far as the continuum excited states contains both proton $1p1h$ configurations and a scattering neutron orbit. This is the case for the resonance peaks around $\epsilon_{\text{kin}} = 2.2$ and 3.0 MeV (corresponding to 2^+ states at excitation energy at $E = 4.8$ and 5.6 MeV), and the broad peaks around $\epsilon_{\text{kin}} \approx 10$ MeV and $\epsilon_{\text{kin}} \approx 15 - 22$ MeV, which correspond to the ISGQR and IVGQR, respectively.

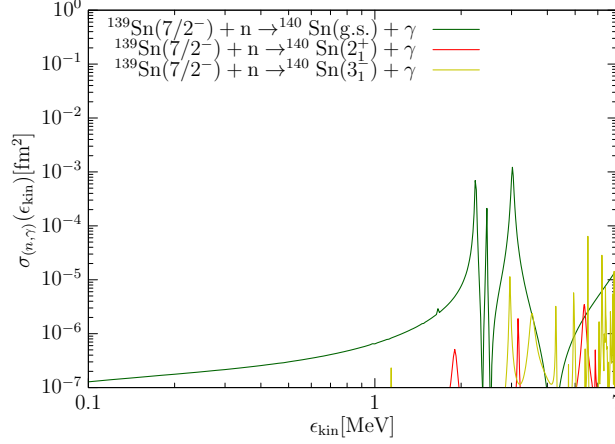


FIG. 11. The calculated (n, γ) cross sections for $^{139}\text{Sn}(7/2^-) + n \rightarrow ^{140}\text{Sn}$ with E2 transitions populating different low-lying states in ^{140}Sn ; the ground state (plotted with a green curve), the low-lying 2_1^+ states (red curve), and the octupole vibrational state 3_1^- (yellow curve). The horizontal axis is the neutron kinetic energy ϵ_{kin} . The cross section for 2_2^+ is not seen as it is smaller than the plotted range. The smoothing parameter is $\eta = 10^{-5}$ MeV.

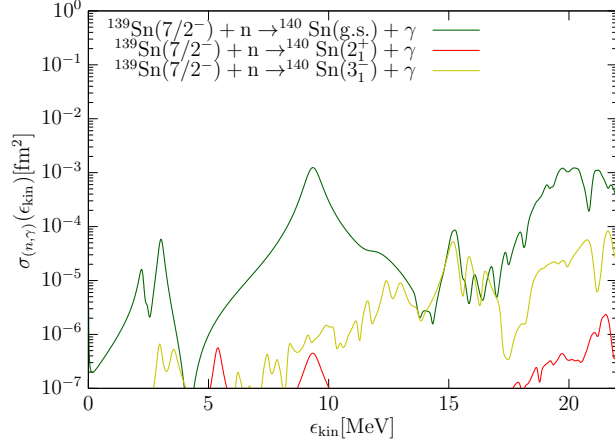


FIG. 12. The same as Fig. 11, but for higher neutron kinetic energy and larger smoothing parameter $\eta = 0.1$ MeV.

IV. CONCLUSION

The continuum random-phase approximation (cRPA) with use of the Green's function in the coordinate-space representation enables us to describe various types of correlated particle-hole excitations and their coupling to unbound single-particle orbits. Utilizing this feature of the cRPA, we have formulated a quantum many-body theory to calculate the cross section of the radiative neutron capture reaction on neutron-rich nuclei with a scope

of application to the r-process nucleosynthesis. We have given, in our previous publication [40], a formulation for the (n, γ) reaction, in which the final state of the gamma transition is restricted to the ground state of an even-even nucleus. In the present study, we have introduced an extended formulation so that we can describe decay channels in which the gamma transition populates low-lying excited states. With the cRPA approach it is possible to describe various excitation modes present in the scattering state of $n + (A - 1)$, including soft dipole excitation, the giant resonances as well as non-collective excitations and the single-particle resonances. Furthermore, we are able to take into account the correlation in the final states of the gamma transition, e.g. the low-lying quadrupole and octupole vibrational states.

In order to demonstrate the new features taken into account in the cRPA description of the (n, γ) reaction, we have performed numerical study of the neutron capture of neutron-rich nucleus ^{139}Sn followed by E1 or E2 γ transitions to the ground state or low-lying excited states $2_1^+, 2_2^+$ and 3_1^- in ^{140}Sn . The RPA correlation in the scattering states produces resonance structures in the (n, γ) cross section, which originates from particle-hole excitations with both collective and non-collective characters. There appear resonances with rather wide widths, arising from single-particle resonances and collective excitations such as the giant resonances. In addition narrow resonances emerge from non-collective excitation modes, which are particle-hole excitations from bound to bound orbits of neutrons as well as those of protons. The correlation in the final states, i.e. the low-lying quadrupole and octupole states ^{140}Sn , has also significant impact on the (n, γ) cross section. A particular example is the transitions to the 3_1^- state, which is not present in the single-particle model as this collective state appears below the neutron separation energy only by including the RPA correlation. Furthermore additional neutron partial waves contribute to the capture, compared with those in the single-particle model, because of the strong configuration mixing of many one-particle-one-hole states in the 3_1^- state.

Finally we remark a scope for future developments of the present study. The pair correlation neglected in the present formulation can be taken into account by a straightforward extension from the cRPA to the continuum quasiparticle random-phase approximation (cQRPA). This will be done by combining the formulation in Ref. [40] and that in the present study. This extension will make it possible to describe the (n, γ) reaction systematically for open-shell spherical nuclei. Extension of the model space to that beyond the RPA, including

many-particle many-hole states, is another direction of future development, which might be required for description of the neutron capture in nuclei close to the stability line, e.g. in application to the s-process and capture reactions at high neutron energy. Description of the case where the final state nucleus is an odd- A or an odd-odd nucleus also need to be studied in future.

V. ACKNOWLEDGMENTS

The authors thank Kazuyuki Sekizawa and Kenichi Yoshida for valuable discussions. This work was supported by the JSPS KAKENHI (Grant No. 20K03945).

Appendix A: T matrix for (γ, n) reaction

We shall discuss a relation between the T matrix $T_{(\gamma, n)}^{\text{RPA}} = \langle ph | \hat{V}_{\text{scf}}(\hat{F}; \omega) | 0 \rangle$ given in the present cRPA theory and the T matrix of the (γ, n) reaction in the general theory of nuclear reaction.

Following the general reaction theory [49], the T matrix for the (γ, n) reaction in the prior form is given by

$$T_{(\gamma, n)} = \langle \Psi_{n+(A-1)}^{(-)}(E) | \hat{M} | \Psi_{i, A} \rangle, \quad (\text{A1})$$

$$|\Psi_{n+(A-1)}^{(-)}(E)\rangle = |\phi_n \Psi_{A-1}\rangle + \hat{G}^{(-)}(E) \hat{V} |\phi_n \Psi_{A-1}\rangle, \quad (\text{A2})$$

for the gamma-ray absorption caused by the multipole field \hat{M} with a kinematical factor and the angular momentum omitted. Here $|\Psi_{i, A}\rangle$ is the target nucleus A at state i and $|\phi_n \Psi_{A-1}\rangle$ is the final state in the $n + (A - 1)$ channel consisting of an escaping neutron ϕ_n and the daughter nucleus $(A - 1)$ (the state Ψ_{A-1}). $|\Psi_{n+(A-1)}^{(-)}(E)\rangle$ is an energy eigenstate with an incoming boundary condition, which is given as a solution of the Lippman-Schwinger equation. Here \hat{V} is the interaction between the neutron and the subsystem $(A - 1)$, and $\hat{G}^{(\pm)}(E)$ is a many-body Green's function $\hat{G}^{(\pm)}(E) = \frac{1}{E - \hat{H} \pm i\eta}$ for the total Hamiltonian $\hat{H} = \hat{H}_0 + \hat{V}$ with \hat{H}_0 describing non-interacting $n + (A - 1)$ system. Note that the T matrix can be written also as

$$T_{(\gamma, n)} = \langle \phi_n \Psi_{A-1} | \hat{M} | \Psi_{i, A} \rangle + \langle \phi_n \Psi_{A-1} | \hat{V} \hat{G}^{(+)}(E) \hat{M} | \Psi_{i, A} \rangle \quad (\text{A3})$$

which is the post form representation of the T matrix. Besides the photo-nuclear interaction \hat{M} , the interaction \hat{V} also contributes to the T matrix in the post form as represented by the second term in the r.h.s. of Eq.(A3).

The RPA T matrix (c.f. Eqs.(14) and (16)) is written as

$$T_{(\gamma,n)}^{\text{RPA}} = \langle ph | \hat{F} | 0 \rangle + \langle ph | \hat{V}_{\text{ind}}(\hat{F}; \omega) | 0 \rangle \quad (\text{A4})$$

in terms of the induced field

$$\hat{V}_{\text{ind}}(\hat{F}; \omega) = \int dx \frac{\delta \hat{U}(x)}{\delta \rho} \delta \rho(x, \omega), \quad \frac{\delta \hat{U}(x)}{\delta \rho} = \frac{\delta U(x)}{\delta \rho} \hat{\rho}(x). \quad (\text{A5})$$

The first and second terms in Eq.(A4) correspond to the respective terms in Eq.(A3). To see this, we first note correspondence in the initial and final states:

$$\langle ph | \leftrightarrow \langle \phi_n \Psi_{A-1} |, \quad \hat{O}_i^\dagger | 0 \rangle \leftrightarrow | \Psi_{i,A} \rangle \quad (\text{A6})$$

assuming the excited state $| \Psi_{i,A} \rangle$ of the nucleus A is described by the RPA creation operator \hat{O}_i^\dagger acting on the ground state $| 0 \rangle$ in the static selfconsistent field. The particle-hole state $| ph \rangle = a_p^\dagger a_h | 0 \rangle$ corresponds to the scattering final state $| \phi_n \Psi_{A-1} \rangle$ if we assign the daughter nucleus Ψ_{A-1} as a one-hole state $a_h | 0 \rangle$ whereas the particle a_p^\dagger to the neutron scattering wave ϕ_n . We see then correspondence

$$\langle ph | \hat{F} | 0 \rangle = \langle ph | \hat{M} | i \rangle \leftrightarrow \langle \phi_n \Psi_{A-1} | \hat{M} | \Psi_{i,A} \rangle \quad (\text{A7})$$

between the first terms in the r.h.s. of Eq.(A4) and (A3). See also Fig.1(a).

Concerning the second term of the RPA T matrix, the induced field

$$\hat{V}_{\text{ind}}(\omega) = \int dx \frac{\delta U(x)}{\delta \rho} \hat{\rho}(x) \delta \rho(x, \omega) \quad (\text{A8})$$

is a mean-field part of the RPA residual interaction $\hat{V}_{\text{RPA}} = \frac{1}{2} \int dx \frac{\delta U(x)}{\delta \rho} \hat{\rho}(x) \hat{\rho}(x)$. It is associated with the perturbation represented by the density response $\delta \rho(x, \omega)$, which is brought by the action $\hat{F} = [\hat{M}, \hat{O}_i^\dagger]$ of the multipole field \hat{M} on the initial state $\hat{O}_i^\dagger | 0 \rangle$. We thus see a correspondence

$$\hat{V}_{\text{ind}}(\hat{F}; \omega) | 0 \rangle \leftrightarrow \hat{V} \hat{G}^{(+)}(E) \hat{M} | \Psi_{i,A} \rangle \quad (\text{A9})$$

under an approximation that the interaction \hat{V} is replaced by the RPA residual interaction \hat{V}_{RPA} and the model space is limited to the one-particle-one-hole subspace. Thus we find

that the second terms in the r.h.s. of Eq.(A4) and (A3) corresponds to each other:

$$\langle ph | \hat{V}_{\text{ind}}(\hat{F}; \omega) | 0 \rangle \leftrightarrow \langle \phi_n \Psi_{A-1} | \hat{V} \hat{G}^{(+)}(E) \hat{M} | \Psi_{i,A} \rangle. \quad (\text{A10})$$

It is noted also that the general form of the T matrix and the RPA T matrix have a similar structure; the interaction \hat{V} or \hat{V}_{RPA} are taken into account up to infinite order as

$$T_{(\gamma,n)} = \langle \phi_n \Psi_{A-1} | \left(\hat{M} + \hat{V} \hat{G}_0^{(+)}(E) \hat{M} + \hat{V} \hat{G}_0^{(+)}(E) \hat{V} \hat{G}_0^{(+)}(E) \hat{M} + \dots \right) | \Psi_{i,A} \rangle, \quad (\text{A11})$$

$$T_{(\gamma,n)}^{\text{RPA}} = \langle ph | \left(\hat{F} + \frac{\delta \hat{U}}{\delta \rho} R_0(\omega) F + \frac{\delta \hat{U}}{\delta \rho} R_0(\omega) \frac{\delta U}{\delta \rho} R_0(\omega) F + \dots \right) | 0 \rangle \quad (\text{A12})$$

where the density response $\delta\rho(x, \omega)$ obeying the linear response equation (9) is symbolically represented as Eq.(17). Here $\hat{G}_0^{(+)}(E) = \frac{1}{E - \hat{H}_0 + i\eta}$ is the unperturbed Green's function whereas $R_0(\omega)$ is the unperturbed response function Eq.(11). A diagrammatic representation is shown in Fig.1.

Appendix B: The (γ, n) cross section under spherical symmetry

The self-consistent field $\hat{V}_{LM}^{\text{scf}}(\omega) = \hat{F}_{LM} + \hat{V}_{LM}^{\text{ind}}(\omega)$ is a rank L non-local one-body operator. The radial coordinate representation of this matrix element is expressed as

$$v_{L,l'j',lj}^{\text{scf}}(r_x, r_y, \omega) = F_{L,l'j',lj}(r_x, r_y) + \langle l' j' | |Y_L| | l j \rangle \frac{\delta U}{\delta \rho}(r_x) \frac{1}{r_x^2} \delta\rho_L(r_x, \omega) \delta(r_x - r_y). \quad (\text{B1})$$

The radial matrix element $F_{L,l'j',lj}(r_x, r_y)$ of the operator \hat{F}_{LM} is given in Eq.(34) of Ref. [41].

Inserting Eq.(B1) into Eq.(22), we obtain

$$\begin{aligned}
\sigma_{iL_i+\gamma\rightarrow[\epsilon l_p j_p h]_L}^\lambda(E_\gamma) &= -\frac{f(E_\gamma)}{\pi(2L_i+1)} \\
&\times \text{Im} \left\{ |\langle l_p j_p | Y_L | l_h j_h \rangle|^2 \iint dr_x dr_{x'} \phi_{n_h l_h j_h}^*(r_x) \frac{\delta U}{\delta \rho}(r_x) \frac{1}{r_x^2} \delta \rho_L^*(r_x, \omega_\gamma + \omega_i) \right. \\
&\quad \times G_{0c, l_p j_p}(r_x, r_{x'}, \epsilon_h + \hbar\omega_\gamma + \hbar\omega_i + i\eta) \frac{\delta U}{\delta \rho}(r_{x'}) \frac{1}{r_{x'}^2} \delta \rho_L(r_{x'}, \omega_\gamma + \omega_i) \phi_{n_h l_h j_h}(r_{x'}) \\
&+ \langle l_p j_p | Y_L | l_h j_h \rangle^* \iiint dr_x dr_{x'} dr_{y'} \phi_{n_h l_h j_h}^*(r_x) \frac{\delta U}{\delta \rho}(r_x) \frac{1}{r_x^2} \delta \rho_L^*(r_x, \omega_\gamma + \omega_i) \\
&\quad \times G_{0c, l_p j_p}(r_x, r_{x'}, \epsilon_h + \hbar\omega_\gamma + \hbar\omega_i + i\eta) F_{L, l_p j_p, l_h j_h}(r_{x'}, r_{y'}) \phi_{n_h l_h j_h}(r_{y'}) \\
&+ \langle l_p j_p | Y_L | l_h j_h \rangle \iiint dr_x dr_y dr_{x'} \phi_{n_h l_h j_h}^*(r_y) F_{L, l_p j_p, l_h j_h}^*(r_x, r_y) \\
&\quad \times G_{0c, l_p j_p}(r_x, r_{x'}, \epsilon_h + \hbar\omega_\gamma + \hbar\omega_i + i\eta) \frac{\delta U}{\delta \rho}(r_{x'}) \frac{1}{r_{x'}^2} \delta \rho_L(r_{x'}, \omega_\gamma + \omega_i) \phi_{n_h l_h j_h}(r_{x'}) \\
&+ \iiint dr_x dr_y dr_{x'} dr_{y'} \phi_{n_h l_h j_h}^*(r_y) F_{L, l_p j_p, l_h j_h}^*(r_x, r_y) \\
&\quad \left. \times G_{0c, l_p j_p}(r_x, r_{x'}, \epsilon_h + \hbar\omega_\gamma + \hbar\omega_i + i\eta) F_{L, l_p j_p, l_h j_h}(r_{x'}, r_{y'}) \phi_{n_h l_h j_h}(r_{y'}) \right\}. \tag{B2}
\end{aligned}$$

The function $G_{0c, l_p j_p}(r_x, r_{x'}, \epsilon)$ is the single-particle Green's function G_{0c} in the partial wave $l_p j_p$. It is calculated exactly using Eq.(B2) of Ref. [41], together with the subtraction of the bound orbits, see Eq.(20). The correlation in the low-lying state $|iL_i M_i\rangle$ is reflected in $F_{L, l' j', l_j}$ while the correlation in the continuum RPA states $|kLM(E)\rangle$ is in the density fluctuation $\delta\rho_L$.

-
- [1] E. M. Burbidge, G. R. Burbidge, W. A. Fowler, and F. Hoyle, *Rev. Mod. Phys.* **29**, 547 (1957).
 - [2] M. Arnould, S. Goriely, and K. Takahashi, *Phys. Rep.* **450**, 97 (2007).
 - [3] J. J. Cowan, C. Sneden, J. E. Lawler, A. Aprahamian, M. Wiescher, K. Langanke, G. Martinez-Pinedo, and F.-K. Thielemann, *Rev. Mod. Phys.* **93**, 015002 (2021).
 - [4] B. P. Abbott *et al.*, *Phys. Rev. Lett.* **119**, 161101 (2017).
 - [5] B. P. Abbott *et al.*, *Astrophys. J. Lett.* **848**, L12 (2017).
 - [6] E. Pian *et al.*, *Nature* **551**, 67 (2017).
 - [7] D. Kasen, B. Metzger, J. Barnes, E. Quataert, and E. Ramirez-Ruiz, *Nature* **551**, 80 (2017).
 - [8] V. A. Villar *et al.*, *Astrophys. J. Lett.* **851**, L21 (2017).

- [9] W. Hauser and H. Feshbach, *Phys. Rev.* **87**, 366 (1952).
- [10] G. J. Mathews, A. Mengoni, F.-K. Thielemann, and W. A. Fowler, *Astrophys. J.* **270**, 740 (1983).
- [11] A. M. Lane and J. E. Lynn, *Nucl. Phys.* **17**, 563 (1960).
- [12] S. Raman, R. F. Carlton, J. C. Wells, E. T. Journey, and J. E. Lynn, *Phys. Rev. C* **32**, 18 (1985).
- [13] A. Mengoni, T. Otsuka, and M. Ishihara, *Phys. Rev. C* **52**, R2334 (1995).
- [14] T. Rauscher, R. Bieber, H. Oberhummer, K.-L. Kratz, J. Dobaczewski, P. Möller, and M. M. Sharma, *Phys. Rev. C* **57**, 2031 (1998).
- [15] L. Bonneau, T. Kawano, T. Watanabe, and S. Chiba, *Phys. Rev. C* **75**, 054618 (2007).
- [16] S. Chiba, H. Koura, T. Hayakawa, T. Maruyama, T. Kawano, and T. Kajino, *Phys. Rev. C* **77**, 015809 (2008).
- [17] T. Rauscher, *Nucl. Phys. A* **834**, 635c (2010).
- [18] Y. Xu and S. Goriely, *Phys. Rev. C* **86**, 045801 (2012).
- [19] Y. Xu, S. Goriely, A. J. Koning, and S. Hilaire, *Phys. Rev. C* **90**, 024604 (2014).
- [20] S.-S. Zhang, J.-P. Peng, M. S. Smith, G. Arbanas, and R. L. Kozub, *Phys. Rev. C* **91**, 045802 (2015).
- [21] K. Sieja and S. Goriely, *Eur. Phys. J. A* **57**, 110 (2021).
- [22] I. Tanihata, H. Hamagaki, O. Hashimoto, Y. Shida, N. Yoshikawa, K. Sugimoto, O. Yamakawa, T. Kobayashi, and N. Takahashi, *Phys. Rev. Lett.* **55**, 2676 (1985).
- [23] P. G. Hansen and B. Jonson, *Europhys. Lett.* **4**, 409 (1987).
- [24] Y. Suzuki, K. Ikeda, and H. Sato, *Prog. Theor. Phys.* **83**, 180 (1990).
- [25] G. F. Bertsch and H. Esbensen, *Ann. Phys. A* **209**, 327 (1991).
- [26] N. Paar, D. Vretenar, E. Khan, and G. Colò, *Rep. Prog. Phys.* **70**, 691 (2007).
- [27] I. Tanihata, H. Savajols, and R. Kanungo, *Prog. Part. Nucl. Phys.* **68**, 215 (2013).
- [28] S. Goriely, *Phys. Lett. B* **436**, 10 (1998).
- [29] S. Goriely and E. Khan, *Nucl. Phys.* **A706**, 217 (2002).
- [30] S. Goriely, E. Khan, and M. Shamyn, *Nucl. Phys. A* **739**, 331 (2004).
- [31] E. Litvinova, H. P. Loens, K. Langanke, G. Martínez-Pinedo, T. Rauscher, P. Ring, F.-K. Thielemann, and V. Tselyaev, *Nucl. Phys. A* **823**, 26 (2009).
- [32] A. Avdeenkov, S. Goriely, S. Kamerdzhiev, and S. Krewald, *Phys. Rev. C* **83**, 064316 (2011).

- [33] I. Daoutidis and S. Goriely, *Phys. Rev. C* **86**, 034328 (2012).
- [34] M. Martini, S. Péru, S. Hilaire, S. Goriely, and F. Lechaftois, *Phys. Rev. C* **94**, 014304 (2016).
- [35] S. Typel and G. Baur, *Nucl. Phys. A* **759**, 247 (2005).
- [36] S. Shlomo and G. F. Bertsch, *Nucl. Phys. A* **243**, 507 (1975).
- [37] G. F. Bertsch and S. F. Tsai, *Phys. Rep.* **18**, 125 (1975).
- [38] M. Matsuo, *Nucl. Phys. A* **696**, 371 (2001).
- [39] T. Nakatsukasa, K. Matsuyanagi, M. Matsuo, and K. Yabana, *Rev. Mod. Phys.* **88**, 045004 (2016).
- [40] M. Matsuo, *Phys. Rev. C* **91**, 034604 (2015).
- [41] T. Saito and M. Matsuo, *Phys. Rev. C* **104**, 034305 (2021).
- [42] A. Zangwill and P. Soven, *Phys. Rev. A* **21**, 1561 (1980).
- [43] P. Ring and P. Schuck, *The Nuclear Many-Body Problem* (Springer-Verlag, Berlin, 1980).
- [44] C. A. Bertulani and P. Danielewicz, *Introduction to Nuclear Reaction* (Institute of Physics Publishing, London, 2004).
- [45] I. J. Thompson and F. M. Nunes, *Nuclear Reactions for Astrophysics* (Cambridge University Press, Cambridge, 2004).
- [46] T. Nakatsukasa and K. Yanaba, *J. Chem. Phys.* **114**, 2550 (2001).
- [47] Mass explorer, <http://massexplorer.frib.msu.edu/content/DFTMassTables.html>.
- [48] H. Shimoyama and M. Matsuo, *Phys. Rev. C* **88**, 054308 (2013).
- [49] J. R. Taylor, *Scattering Theory: The Quantum Theory of Nonrelativistic Collisions* (Dover Publications, New York, 2006).